



Characteristics of low-latitude Pc1 pulsations during geomagnetic storms

J. Bortnik,^{1,2} J. W. Cutler,^{2,3} C. Dunson,² T. E. Bleier,² and R. L. McPherron⁴

Received 9 October 2007; revised 6 November 2007; accepted 14 December 2007; published 3 April 2008.

[1] We use search-coil magnetometer data from a low-latitude station in Parkfield, California ($L = 1.77$) to study the occurrence of Pc1 pulsations associated with geomagnetic storms. The Pc1 pulsations and storms are identified using automatic algorithms, and the statistical distributions are examined using a superposed epoch analysis technique, as a function of local time, time relative to storm main phase, and storm intensity. Results show that Pc1 pulsations are 2–3 times more likely (than normal) to be observed in the 2–4 d following moderate storms and 4–5 times more likely in the 2–7 d following intense storms. The Pc1 frequencies are higher in moderate storms than they are in nonstorm times and become even higher and occupy a greater range of local times as the strength of the storms increase. These results are consistent with the idea that the source of EMIC waves extends to lower L values as storm intensity increases.

Citation: Bortnik, J., J. W. Cutler, C. Dunson, T. E. Bleier, and R. L. McPherron (2008), Characteristics of low-latitude Pc1 pulsations during geomagnetic storms, *J. Geophys. Res.*, 113, A04201, doi:10.1029/2007JA012867.

1. Introduction

[2] Pc1 pulsations consist of electromagnetic ion cyclotron (EMIC) waves in the range 0.2–5 Hz that are observed on the ground. Such EMIC waves are believed to be generated in the equatorial region of the magnetosphere at $L \sim 4$ –8 [Anderson *et al.*, 1992] due to unstable distributions of ring current ions [Cornwall, 1965]. They propagate roughly along the magnetic field line in the left-hand mode, enter the high-latitude ionosphere, and are mode-converted into the right-hand mode. They then propagate horizontally and isotropically in the ionospheric waveguide [e.g., Fraser, 1968; Manchester, 1966, 1968; Jacobs, 1970, p. 115], which is centered on the F2 region electron density maximum at ~ 350 km [Manchester, 1966]. The wave power progressively attenuates and leaks to the ground as it propagates from high to low latitudes, the attenuation being most severe during the daytime [Althouse and Davis, 1978], resulting in a nighttime occurrence maximum at low latitudes [e.g., Jacobs, 1970, p. 28].

[3] Past studies have shown that Pc1 pulsations at low latitudes maximize in the 2–7 d following the storm main phase [Wentworth, 1964; Heacock and Kivinen, 1972]. The number, frequency, and diurnal distribution of pulsations depends on a variety of factors including solar cycle phase, storm intensity, observation latitude, time after main phase,

and pulsation type (structured/unstructured) [e.g., Kerttula *et al.*, 2001a, 2001b]. Recent statistical studies using long data sets have confirmed that structured pulsations at high and middle latitudes redistribute in local time, moving from an occurrence maximum in the early evening, to a maximum in the local dawn [e.g., Kerttula *et al.*, 2001a, 2001b] and increase both in number and frequency a few days after the main phase.

[4] In the present study, an ~ 8 year period of low-latitude magnetometer data is used to study the diurnal distribution of Pc1 pulsations (occurrence and frequency) as a function of time relative to geomagnetic storms. We use novel algorithms that identify both geomagnetic storms and Pc1 pulsations according to well-defined criteria. In addition, we compare the distribution of storm-time Pc1 pulsations against the distribution of all identified Pc1 pulsations, as well as strictly nonstorm-time pulsations, in order to quantify how storm-time distributions deviate relative to normal and quiet times. In section 2 we discuss the data and our automatic identification algorithms, section 3 presents our statistical results, and section 4 discusses the findings of this work.

2. Data Description and Identification Procedure

2.1. Storm Identification

[5] The geomagnetic storms in the present study were identified using the D_{st} index (courtesy of World Data Center for Geomagnetism, Kyoto University). This particular index was used because it closely reflects the dynamics of the energetic ions in the ring current, believed to be the source of EMIC waves (and hence Pc1 pulsations on the ground). Our aim is to detect isolated storms that have an initial quiet period, a well-defined (and temporally contained) active period, followed by a final quiet period. The D_{st} index for one of the most intense storms on record

¹Department of Atmospheric and Oceanic Sciences, University of California, Los Angeles, California, USA.

²Department of Aeronautics and Astronautics, Space Systems Development Laboratory, Stanford University, Palo Alto, California, USA.

³QuakeFinder, LLC, Palo Alto, California, USA.

⁴Institute of Geophysics and Planetary Physics, University of California, Los Angeles, California, USA.

(20 November 2003) is shown in Figure 1 together with a spectrogram of our magnetometer data, and our algorithm is illustrated in Figure 1b which proceeds in three broad steps:

[6] 1. We search for active periods, which we define as $D_{st} < -50$ nT, that are “isolated,” i.e., each active period is surrounded by quiet periods (which we define as $D_{st} > -35$ nT) for longer than 5 d. In each such active, isolated period, the minimum D_{st} value (D_{st}^{\min}) is found.

[7] 2. For each D_{st}^{\min} , a “quiet” threshold (A_q) is identified as the minimum of $0.35D_{st}^{\min}$, or -35 nT, and a “stormy” threshold (A_{st}) is identified as the minimum of $0.5D_{st}^{\min}$, or -50 nT. The D_{st} time series is smoothed with a 9-h sliding-average window (red curve in Figure 1b), and the times of threshold crossing are identified as shown in Figure 1b.

[8] 3. In order to be considered a “clean,” isolated storm (referring to the parameters defined in Figure 1b), we require that $\Delta t_{q1} \geq 3$ d, $\Delta t_{q2} \geq 6$ d, $\Delta t_{st} \leq 2$ d, and that the transition between stormy and quiet phases be smooth, i.e., $\partial D_{st}/\partial t (t_{q1}^{(1)}$ to $t_{st}^{(0)}) < 0$ and $\partial D_{st}/\partial t (t_{st}^{(1)}$ to $t_{q2}^{(0)}) > 0$.

[9] These rather restrictive criteria were adopted to ensure that there would be no other (significant) geomagnetic activity surrounding the identified storm, which may produce their own Pc1 pulsations, and confound our superposed epoch analysis. The above criteria also exclude storms with more than one distinct main phase (e.g., Halloween storm of 30 October 2003) because of the need to have only one distinct fiducial time in the storm period against which the relative timing of Pc1 pulsations will be compared.

2.2. Pc1 Event Identification

[10] The triaxial search-coil magnetometer data used in the present study was recorded at Parkfield, California (Geographic: $(35.945^\circ, -120.542^\circ)$, CGM: $(41.61^\circ, -56.8^\circ)$, dip: 60.2° , declination: 14.7° , L -value: 1.77), in the period February 1999 to July 2006, which covers the period surrounding solar maximum 23 (~ 2000 – 2001), including the period of high-speed streams in the declining phase of the cycle (~ 2002 – 2003). An example of Pc1 pulsations in this high-speed stream period is shown in Figure 1a.

[11] The Pc1 pulsations are automatically identified and characterized with a recently developed algorithm, described in detail by Bortnik *et al.* [2007], where further information on the symbols and derived quantities used in the present paper is provided. This algorithm consists of three broad steps summarized below:

[12] 1. Spectral peaks in a typical dynamic spectrogram are identified, which exceed the daily background median spectrum significantly (by a factor of ~ 10 in our case). Three frequencies are recorded to describe each spectral peak: the bottom ($f_{\text{bot}}^{\text{pk}}$), top ($f_{\text{top}}^{\text{pk}}$), and the frequency containing maximum wave power ($f_{\text{max}}^{\text{pk}}$).

[13] 2. The spectral peaks in consecutive time segments in the dynamic spectrogram are grouped together to form individual events. Spectral peaks need to satisfy a “spectral overlap” criterion, and be of a certain minimum duration (10 min in our case) to be counted as an event. We note that

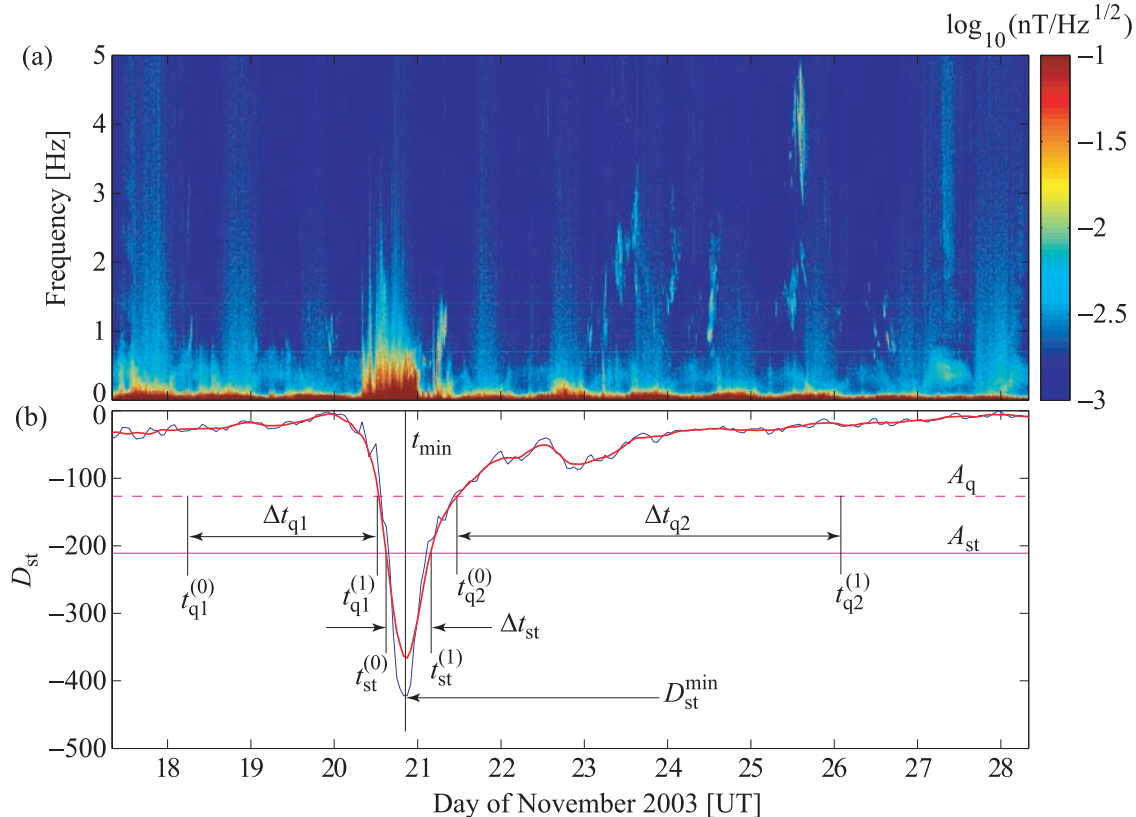


Figure 1. Example of Pc1 pulsations associated with the 20 November 2003 storm. (a) Dynamic spectrogram of X-component of magnetic field, and (b) D_{st} index showing storm development and storm identification threshold values.

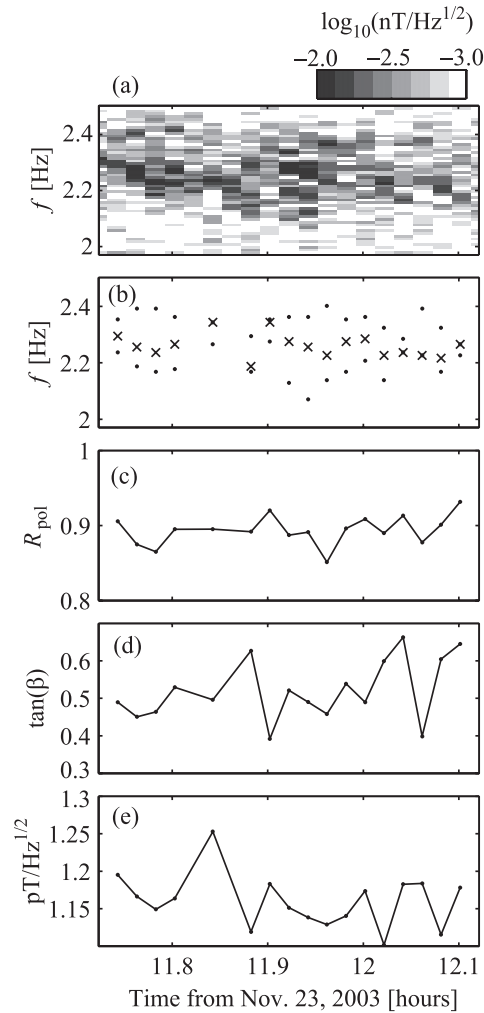


Figure 2. Example of an individual, identified Pc1 event on 23 November 2003. (a) Spectrogram of identified Pc1 event, (b) $f_{\text{bot}}^{\text{pk}}$ (lower dot), $f_{\text{top}}^{\text{pk}}$ (upper dot), and $f_{\text{max}}^{\text{pk}}$ (crosses) as a function of time, (c) polarization ratio R_{pol} , (d) ellipticity ratio, and (e) band-averaged power spectral density.

typical Pc1 events have durations from fractions of an hour, to several hours, and spectral peaks shorter than 10 min are considered to be spurious noise in our analysis and discarded.

[14] 3. The full set of polarization parameters (e.g., polarization ratio R_{pol} , ellipticity $\tan(\beta)$, sense of rotation ($\text{sign}(\beta)$), major axis orientation ($\tan(\theta_{\text{ax}})$), and wave normal angles (θ_k , ϕ_k) are extracted for each of the identified wave events, and recorded as a function of time.

[15] An example of a single, automatically identified event on 23 November 2003 is shown in Figure 2. The dynamic spectrogram showing the Pc1 pulsation to be identified is shown in Figure 2a, the scaled frequency-time ($f-t$) characteristics are plotted in Figure 2b, where the upper and lower dots represent $f_{\text{top}}^{\text{pk}}$, and $f_{\text{bot}}^{\text{pk}}$, and the crosses represent $f_{\text{max}}^{\text{pk}}$ within each spectral band. The polarization ratio R (i.e., fraction of polarized power in the wave relative to the total power) is shown in Figure 2c, the ellipticity (ratio of major axis to the minor axis of the polarization ellipse) in Figure 2d, and total band-averaged power is

shown in Figure 2e. The panels in Figure 2 indicate that the Pc1 event is highly polarized, i.e., rotates in a right-hand sense relative to the local (positively directed) \mathbf{B} -field, and has a band-averaged power spectral density of ~ 1.1 – 1.2 pT/Hz $^{1/2}$.

[16] Although our Pc1 identification algorithm was developed for the full triaxial data set, and we have all three components available for the period under study, in the present work we have chosen to use only the two horizontal channels for Pc1 identification/characterization. This was done because we do not use polarization or orientation information for the present study (which would necessitate the vertical channel), and results in more robust Pc1 identification since the vertical coil is typically more susceptible to local noises and contamination from underground reflections.

2.3. Identification Results

[17] Using the automatic identification algorithms described above, we analyzed the period February 1999 to July 2006, extracting information on storms, associated Pc1 pulsations, and quiet-time Pc1 pulsations.

2.3.1. Identified Storms

[18] Using the algorithm described in section 2.1, 24 “clean” storms were identified, with D_{st} ranging from -422 nT to -61 nT, having a median of -102 nT. These storms were further subdivided for the purposes of our study into 12 moderate storms ($-100 \leq D_{\text{st}}^{\text{min}} < -50$ nT) and 12 intense storms ($D_{\text{st}}^{\text{min}} < -100$ nT). A graphical representation of the identified storms is given in Figure 3, where we show the D_{st} index and monthly averaged sunspot number (courtesy of NGDC/STP) for the entire period under study. The times of identified storms are indicated with red vertical lines (solid line and dashed lines representing intense and moderate storms, respectively), showing that the majority of storms are clustered around the solar maximum, although the entire 8-year period is nevertheless well sampled. More detailed information on the identified storms is provided in Table 1, where we list the date and time of the storm $D_{\text{st}}^{\text{min}}$, i.e., t_{min} , together with $D_{\text{st}}^{\text{min}}$, and the number of associated Pc1 events for each storm. The list is given in chronological order, being subdivided into moderate and intense storms according to the criteria given above.

2.3.2. Identified Pc1 Events

[19] Using the algorithm described in section 2.2, a total of 8913 individual Pc1 events were identified in our ~ 8 year period, having a broad local time (LT) occurrence minimum at ~ 0800 – 1500 and maximum at ~ 2300 – 0400 , consistent with previous studies [Tepley, 1965] and reported earlier [Bortnik et al., 2007]. The mean duration of Pc1 events was ~ 20 min, and $f_{\text{max}}^{\text{pk}}$ ranged from 0.12 to 4.7 Hz, with a median and mean value of 0.44 and 0.8 Hz, respectively.

[20] For the purposes of our study, we extracted three categories of Pc1 events from the total list, those events corresponding to moderate storms, intense storms, and quiet times. There were a total of 453 and 863 Pc1 events associated with moderate and intense storms, respectively, with mean frequencies of 0.57 Hz and 1.01 Hz, mean bandwidths of 0.22 Hz and 0.27 Hz, and mean durations of 18 min and 20 min, respectively.

[21] In order to compare the storm-time events to quiet-time Pc1 events (section 3.2), we scanned the entire list of

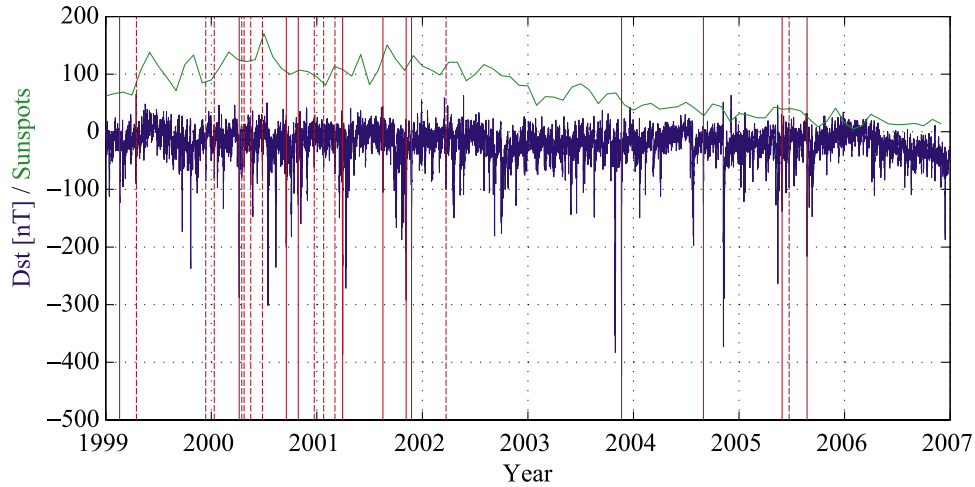


Figure 3. Graphical presentation of geomagnetic storms used in the statistical analysis, shown together with D_{st} index (blue line) and monthly averaged sunspot number to indicate solar cycle phase (green line). The solid and dashed red lines represent the times of intense and moderate storms respectively (see Table 1 for details).

identified Pc1 events, for each event checking the D_{st} values in the few days surrounding the event. If the D_{st} value did not drop below -50 nT for at least 6 d prior to, and for at least 3 d after the recorded event, then the Pc1 event in question was marked as a quiet-time event. In total, 2500 quiet-time Pc1 events were found, with a mean frequency, bandwidth, and duration of 0.65 Hz, 0.21 Hz, and 19 min, respectively. Although the stimulus for these quiet-time Pc1 events was not in the large-scale buildup of the ring current, they are likely associated with a variety of small storms, substorms, pressure pulses in the solar wind, or drifting fluxes of anisotropic protons from the plasma sheet [Olson and Lee, 1983; Kangas et al., 1986; Engebretson et al., 2002].

3. Statistical Results

[22] The relation of Pc1 events to geomagnetic storms was analyzed in two ways: first, the mean values of various Pc1 event parameters were compared against the D_{st}^{\min} of each storm, and second, a superposed epoch analysis was performed, combining separately all intense and moderate storms to identify trends related to t_{\min} and LT.

3.1 D_{st} -Dependent Trends

[23] Using the list of Pc1 events associated with each of our identified storms (listed in Table 1), we calculated the total number of events, their mean duration (in hours), bandwidth (Hz), and mean frequency (Hz) per storm, listed in columns 4–7 of Table 1, respectively. These Pc1 average quantities are plotted in Figure 4, as a function of the storm intensity, D_{st}^{\min} . In order to identify the large-scale trends, we computed a least squares, straight-line fit to the data, shown as the dashed line in each panel. Storm 18 was not included in the linear fits of Figures 4b–4d since there were no Pc1 events associated with this storm.

[24] Figure 4 shows that there is an overall large-scale trend for all four plotted quantities to increase as storm intensity increases, with a clear difference between moderate and intense storms. However, the mean Pc1 quantities

do not vary monotonically as a function of D_{st}^{\min} , and exhibit a significant variance about the overall trend. For example, there are large outliers such as storm 24, whose Pc1 properties are most similar to a storm almost twice its size (storm 21 on 20 November 2003). This variance is attributed to the fact that the Pc1 parameters depend on a variety of factors which control both source and propagation dynamics (e.g., hot and cold magnetospheric ion density and composition, state of the ionospheric waveguide, etc. discussed further in section 3.2), not all of which are controlled by storm intensity in a linear way. It is possible that certain moderate storms could result in enhanced Pc1 generation and/or improved transmission relative to larger storms, particularly when their timing in the solar cycle phase is taken into account [Fraser-Smith, 1970; Mursula et al., 1996].

[25] The trends in Figure 4 show that as storm intensity increases, i.e., D_{st}^{\min} decreases, the total number of Pc1 events recorded at low latitudes increases, and their mean duration, bandwidth, and frequency all tend to increase. This behavior is consistent with the idea that as storm intensity increases, more free energy becomes available in the ring current for the production of EMIC waves, which simultaneously extends to lower L -shells [e.g., Hamilton et al., 1988]. The increase in $f_{\text{hmax}}^{\text{pk}}$, Δf , and Δt could be due to the tendency of EMIC wave frequencies to vary in proportion to the equatorial ion gyrofrequency, such that higher-frequency EMIC waves originate from lower L -shells. In addition, the lower-latitude entry point into the ionosphere results in shorter propagation lengths from the secondary source to our magnetometer and hence less severe damping (especially of the higher-frequency components of the Pc1 pulsation), larger bandwidths, and longer duration [Manchester, 1966, 1968].

3.2. Superposed Epoch Analysis

[26] To study the temporal evolution of the distribution of Pc1 pulsations related to t_{\min} and local time, we performed a superposed epoch analysis as shown in Figure 5. Using the mean local time (LT), and mean universal time (UT) of each

Table 1. Summary of Storms Under Study^a

Number	Time (UT)	D_{st}^{\min} (nT)	Total Pc1's	$\overline{\Delta t}$ (h)	$\overline{\Delta f}$ (Hz)	$\overline{f_{\max}^{\text{pk}}}$ (Hz)
<i>Moderate Storms: $-100 \leq D_{st}^{\min} < -50$ nT</i>						
1	17 Apr 1999 0700	-91	71	0.29483	0.21441	0.69104
2	13 Dec 1999 0900	-85	13	0.34165	0.18858	0.7122
3	11 Jan 2000 2100	-81	14	0.27172	0.21216	0.43926
4	16 Apr 2000 1100	-79	32	0.20477	0.17717	0.45011
5	24 Apr 2000 1400	-61	23	0.21822	0.14400	0.51349
6	17 May 2000 0500	-92	65	0.31224	0.21686	0.67579
7	26 Jun 2000 1700	-76	12	0.19751	0.23143	0.40547
8	23 Dec 2000 0400	-62	9	0.20360	0.13592	0.41047
9	24 Jan 2001 1800	-61	39	0.28088	0.24183	0.51277
10	05 Mar 2001 0200	-73	45	0.27574	0.22937	0.44043
11	24 Mar 2002 0900	-100	47	0.24833	0.25553	0.33178
12	23 Jun 2005 1000	-97	83	0.43050	0.22926	0.72165
<i>Intense Storms: $D_{st}^{\min} < -100$ nT</i>						
13	18 Feb 1999 0900	-123	54	0.32531	0.29116	0.39683
14	07 Apr 2000 0000	-288	44	0.32003	0.24768	0.40248
15	17 Sep 2000 2300	-201	52	0.24628	0.22649	1.00190
16	29 Oct 2000 0300	-127	46	0.28317	0.23061	0.43092
17	31 Mar 2001 0800	-387	79	0.29447	0.25357	0.60509
18	17 Aug 2001 2100	-105	0	—	—	—
19	06 Nov 2001 0600	-292	47	0.39241	0.23871	1.09400
20	24 Nov 2001 1600	-221	34	0.32453	0.22906	1.00970
21	20 Nov 2003 2000	-422	145	0.32114	0.31850	1.37800
22	30 Aug 2004 2200	-126	117	0.39425	0.20626	0.77344
23	30 May 2005 1300	-138	107	0.32202	0.29368	1.18320
24	24 Aug 2005 1100	-216	138	0.35576	0.34074	1.56220

^aThe parameters listed in column order are (1) the storm number, (2) date and time of D_{st}^{\min} (t_{\min}), (3) D_{st}^{\min} , (4) total number of identified Pc1 events associated with the given storm, (5) mean duration (hours), (6) mean bandwidth (Hz), and (7) mean frequency of maximum intensity, f_{\max}^{pk} (Hz).

Pc1 pulsation, we calculate the time of each pulsation relative to the storm t_{\min} , and bin the pulsations into 2 h LT bins (i.e., 12 total LT bins, ordinate of Figure 5), and 12 h relative-time bins (i.e., two bins per day, abscissa of Figure 5). The corresponding LT-integrated (or averaged) line plots are shown in Figure 6 and discussed below.

[27] Figures 5a and 5b show the total number of Pc1 events recorded during moderate and intense storms, respectively. During moderate storms (Figure 5a), there is an increase in the number of Pc1 events on day 0 in the dawn sector, followed by a decrease in the dawn and simultaneous increase on the nightside late on day 0 which shifts towards the local dawn on day 2. The increases are rather modest, are confined to individual bins rather than occurring over extended LT regions, and decay within a few days after t_{\min} (~ 3 , with a few isolated events continuing near days 4–6). In contrast, intense storms (Figure 5b) show a much greater incidence of Pc1 events. There is a peak near day 0 on the dawnside, followed by ~ 1 relatively quiet day and another broad maximum on days 2–7, peaking predominantly on the dawnside, but nevertheless showing significant activity in the night and evening sectors. In both moderate and intense storm events there is a minimum of occurrence during the day. The distributions of Pc1 events for moderate and intense storms (Figures 5a and 5b) have been integrated (summed) over LT and are presented in Figure 6a as the dashed and solid line plots, respectively. The features described above are clearly evident, namely an increase in Pc1 events on day 0, a decrease on day 1, followed by an increase on subsequent days which is storm-intensity-dependent (~ 2 –7 d for intense storms and ~ 2 –5 d for moderate storms).

[28] The features are consistent with previous studies and can be understood as follows: the sharp increase in the

number of Pc1 events near day 0 is associated with the initial (compressional) phase of the storm. Here, the increased solar wind pressure leads to an increase in the

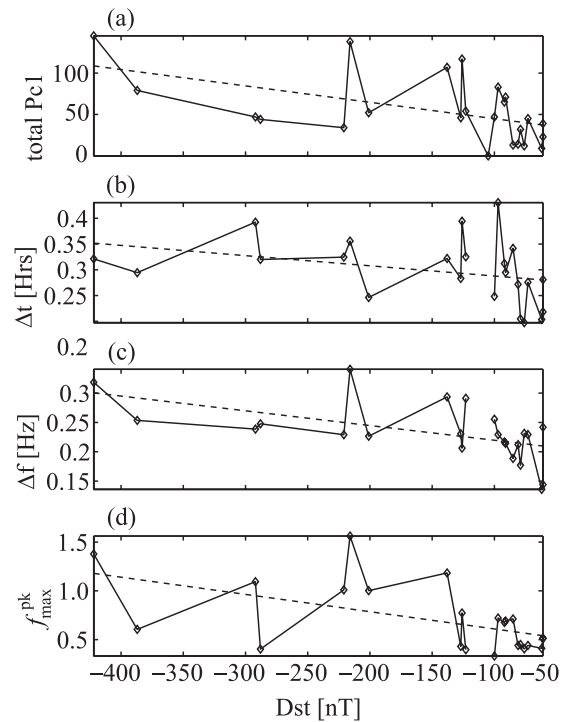


Figure 4. Trend of various Pc1 quantities associated with each storm, as a function of D_{st}^{\min} . (a) Total number of Pc1 events, (b) mean duration (h), (c) mean bandwidth (Hz), and (d) mean f_{\max}^{pk} (see Table 1 for details). The dashed line represents a least-squares fit to the data.

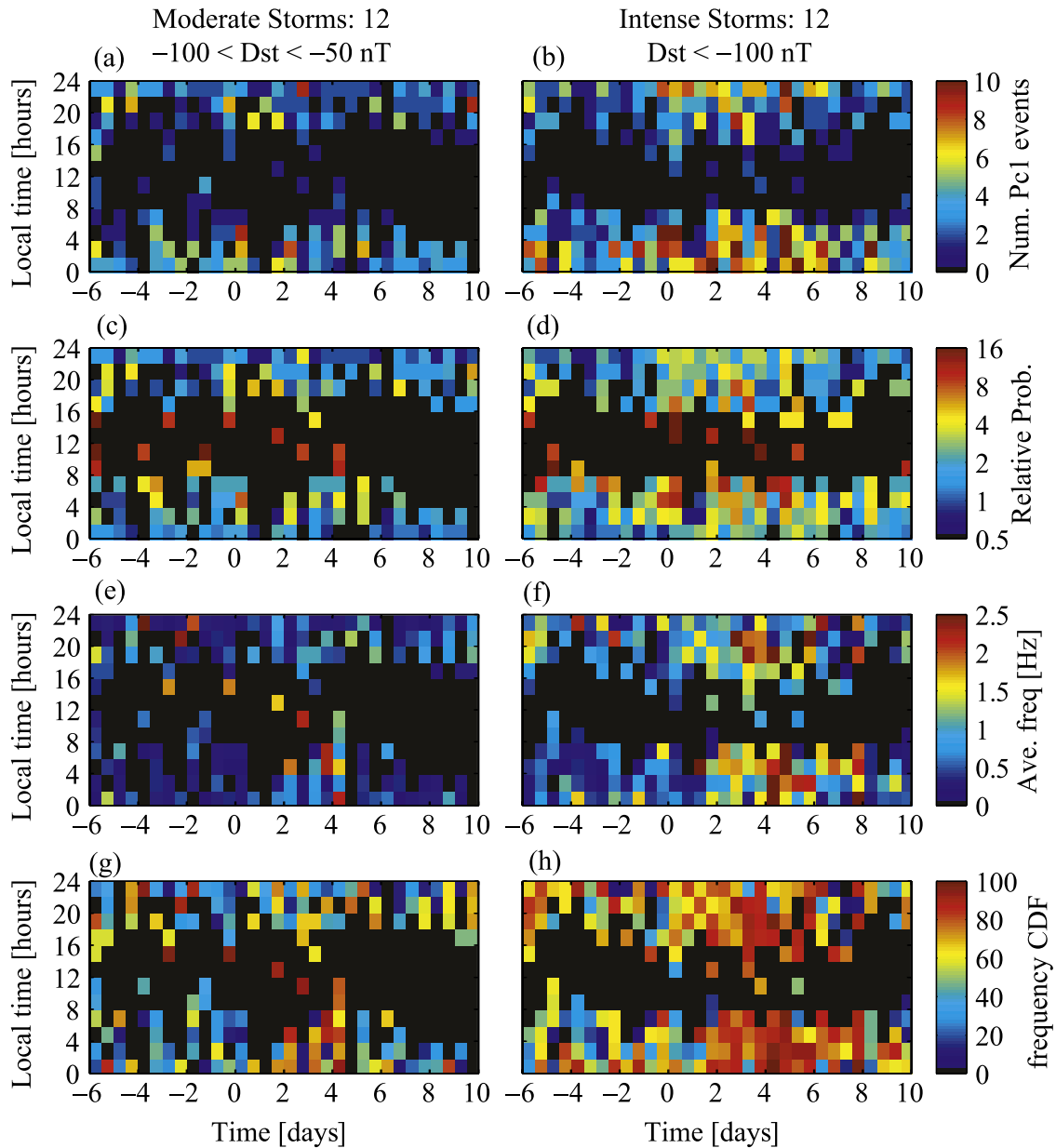


Figure 5. Superposed epoch analysis of Pc1 events relative to moderate (left column) and intense (right column) geomagnetic storms, as a function of local time (ordinate) and time relative to t_{\min} (abscissa). (a), (b) Number of Pc1 events; (c), (d) relative probability of Pc1 observation, compared to nonstorm times; (e), (f) average frequency of observed Pc1 events; (g), (h) long-term probability of observing Pc1 events below the corresponding average-frequency values in Figures 5e and 5f. The black color represents missing data.

proton anisotropy which enhances the production of EMIC waves, particularly on the day side, close to the magnetopause (i.e., high invariant latitudes) [Olson and Lee, 1983; Bräysy et al., 1998]. Such Pc1 events tend to be “unstructured” and maintain a midday maximum when observed at high-latitude ground stations [Anderson and Hamilton, 1993; Kerttula et al., 2001a, 2001b]. The diurnal distribution of Pc1 events changes when observed on low-latitude stations because the EMIC waves propagate in the ionospheric waveguide from their high-latitude entry point to lower latitudes [Manchester, 1966, 1968], and are severely

damped on the day side (particularly at midlatitudes) [e.g., Althouse and Davis, 1978].

[29] The initial period of quiet, followed by the increase of Pc1 events observed in the days following t_{\min} agrees well with similar studies performed at low latitudes [Wentworth, 1964; Heacock and Kivinen, 1972], but the reason for this trend is not fully resolved. It was initially believed that the delay in observed Pc1 activity was related to the EMIC wave generation mechanism [e.g., Heacock and Kivinen, 1972], where the refilling plasmasphere intersected the decaying ring current in the recovery phase of the storm,

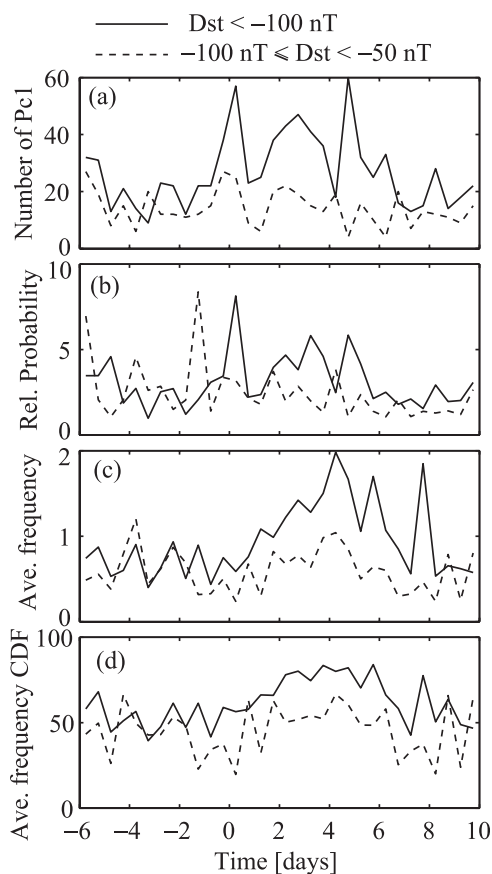


Figure 6. Line plots corresponding to Figure 5, with solid and dashed lines corresponding to intense and moderate storms, respectively. (a) Local-time-integrated plot of Figures 5a and 5b; (b), (c), and (d) Local-time-averaged plots of Figures 5c and 5d, Figures 5e and 5f, and Figures 5g and 5h, respectively.

creating favorable conditions for wave growth [Cornwall, 1965; Cornwall *et al.*, 1970; Fraser-Smith, 1970]. However, a direct association between Pc1 events observed on the ground and EMIC waves in space is difficult to make. Even if EMIC waves were generated during the main phase of the storm, they were not expected to reach the ground due to polarization reversal and reflection at the Buchsbaum frequency [e.g. Rauch and Roux, 1982] together with cyclotron absorption [Horne and Thorne, 1990; Thorne and Horne, 1993, 1994]. Observational results have shown that at least some of the time, there is an unexpectedly favorable correlation between ground and space observations [Perraut *et al.*, 1984], which can be explained by “full-wave” effects, i.e., tunneling and mode-conversion, anticipated in a multi-ion plasma [Johnson and Cheng, 1999]. A satellite-based study of a single, large storm has shown that EMIC wave occurrence maximized in the main phase of the storm [Bräysy *et al.*, 1998], but that the ground observations at the satellite conjugate point did not observe Pc1 pulsations until the late recovery phase. The above work, together with the observation of a similar delay of Pc1 occurrence maxima at middle and high latitudes [Kerttula *et al.*, 2001a, 2001b] suggest that the delayed observation of Pc1 pulsation on the ground is due to improved wave propagation characteristics

in the ionospheric waveguide, in the late recovery phase of storms. We note that the delay to maximum occurrence in our low-latitude data is of the same order as in the midlatitude and high-latitude observations (~ 5 d, Figure 6a), which is also inconsistent with the expanding plasmasphere model.

[30] Next, we compare the results in Figures 5a and 5b to the quiet-time distribution of Pc1 events. The full set of identified quiet-time Pc1 events (c.f. section 2.3.2) from 1999 to 2006 are binned into 2-h LT bins and divided by the total number of quiet days (adjusted by the nonoperational time of the instrument). Quiet days were identified using a similar criterion to the quiet-time Pc1 events. This operation results in a daily probability of quiet-time Pc1 occurrence as a function of LT. Each of the columns in Figures 5a and 5b is normalized by the number of storms (12 each for moderate and intense storms) and multiplied by the number of bins per day (two in our case) to effectively get an average daily occurrence rate binned by LT and relative time. This occurrence rate is then divided by the quiet-time daily probability to get a relative probability of Pc1 occurrence, shown in Figures 5c and 5d. Displaying the data in this manner highlights regions in LT where events are more likely to occur during storm times relative to quiet times, as opposed to simple occurrence numbers, which may hide unusual underlying trends. The corresponding LT-averaged relative probability is shown in Figure 6b.

[31] It is immediately evident from Figures 5c and 5d that even though the number of Pc1 pulsations observed near midday is low (Figures 5a and 5b), they are roughly 8–16 times more likely to occur in association with storms. In Figure 5c, there are a number of Pc1 events in the few days leading up to t_{\min} , which are likely associated with substorms or pressure pulses in the solar wind [Olson and Lee, 1983; Kangas *et al.*, 1986]. Furthermore, as shown by Kangas *et al.* [1986] it is rather surprising that the probability of observing Pc1 pulsations is ~ 5 times higher in association with small pressure pulses, as opposed to large pressure pulses. If we make the rather crude assumption that larger pressure pulses in the solar wind generally lead to more intense storms, than our observations show a consistent trend, namely a larger probability of observing Pc1 pulsations (at midday prior to t_{\min}) in association with moderate storms, rather than strong storms. Figure 5c also shows the gradual motion of an increased probability of Pc1 events from the nightside (days 0, 1) toward the dawnside and day side (days 2–4) similar to high-latitude observations [Kerttula *et al.*, 2001a, 2001b]. For intense storms (Figure 5d) there is a high relative probability of observing Pc1 events near midday on the day of the storm, which was not obvious from Figure 5b. The activity decreases on day 1, but increases significantly on days 2–7 following t_{\min} , in agreement with past work [Wentworth, 1964; Heacock and Kivinen, 1972]. The LT-averaged relative probability (Figure 6b) clearly shows the increased Pc1 events on day 0, followed by a minimum and the gradual maximum in the following few days. The day 0 maximum is likely associated with the compression at the storm onset, as discussed above. Moderate storms show only minor increase in relative probability during days 2–4 (~ 2 – 3), whereas intense storms show a far more pronounced increase on days 2–7 (~ 4 – 5). The moderate storm peak on day –2 results from a single bin at midday, which had 4 Pc1 events, and relative probability of

occurrence well above 16, and is thus not indicative of a large-scale trend.

[32] The frequency of maximum power for each Pc1 event (f_{\max}^{pk}) is calculated by binning it in the same manner as described above, and dividing by the number of Pc1 events observed in the given bin. The results are shown in Figures 5e and 5f, where it is clear that there is an overall increase in the average Pc1 frequency, falling into the range $\sim 1\text{--}4$ Hz (although we saturate the scale at 2.5 Hz for display clarity) in the recovery phase, which is significantly higher than the median and mean frequencies (0.44 and 0.8 Hz). The period of increased frequencies after t_{\min} is $\sim 1.5\text{--}4.5$ d for moderate storms and $\sim 1.5\text{--}8$ d for intense storms. The range of LT in which higher-frequency Pc1 pulsations are observed is also significantly larger for intense storms compared to moderate storms. There appears to be a LT asymmetry in Pc1 frequencies, with higher frequencies observed on the dawnside, which is most likely related to the ionospheric waveguide propagation characteristics and is consistent with previous observations [Campbell and Stiltner, 1965]. The LT-averaged mean frequency plots in Figure 6c show that the mean frequencies are a factor of ~ 2 higher in the aftermath of intense storms, compared to moderate storms.

[33] We compare the average Pc1 pulsation frequencies in Figures 5e and 5f to the long-term distribution as follows: the frequencies f_{\max}^{pk} of the full set of identified Pc1 pulsations from 1999 to 2006 are grouped into 2-h LT bins and are sorted in ascending order. Each of the average frequency values in Figures 5e and 5f is compared against the sorted distribution in its specific LT bin, and its rank is calculated, divided by the total number of Pc1 events in the LT bin and multiplied by 100. This technique provides a measure of where the frequency is located in the cumulative distribution function (CDF), and hence the probability that any Pc1 event will have a frequency lower than the given frequency (e.g., 25%, 50%, and 75% give the first quartile, median, and third quartiles.). The results are displayed in Figures 5g and 5h and show that the frequencies of Pc1 pulsations increase into the 60%–90% range on days 1–5 for moderate storms, but for intense storms are frequently above 90%, and occasionally reach 100%. Thus, the highest frequency Pc1 pulsations observed in the period 1999–2006 occur in association with the most intense storms in the same period. The LT-averaged CDF plots in Figure 6d highlight the difference between the moderate and intense storms.

4. Conclusions

[34] Using data from a low-latitude search coil magnetometer at $L = 1.77$, and a newly developed Pc1 automatic identification algorithm, all the Pc1 pulsations in the period February 1999 to July 2006 were detected and characterized. A number of isolated geomagnetic storms were then identified in the same period using an automatic selection algorithm, and grouped with the Pc1 pulsations occurring within -6 to $+10$ days of the time of D_{st} minimum. A number of statistical analyses were performed, including a superposed epoch analysis as a function of LT, time relative to the minimum D_{st} (t_{\min}), and further parameterized by storm intensity.

[35] It was found that the number of Pc1 pulsations, their mean duration, bandwidth, and peak frequency all increased with increasing storm intensity, albeit with considerable variance. Superposed epoch analysis showed that the total number of Pc1 pulsations, and the time at which the distribution maximized after t_{\min} increased with the intensity of the storm. The diurnal distribution peaked in the late evening in the early recovery phase, and shifted to the early morning in the late recovery. When compared to the quiet-time Pc1 distribution, it was found that Pc1 pulsations were $\sim 2\text{--}3$ times more likely to be observed in the 2–4 d following the t_{\min} of moderate storms, but $\sim 4\text{--}5$ times more likely to be observed in the 2–7 d following the t_{\min} of intense storms, relative to the quiet-time occurrence probability. Daytime Pc1 pulsation observations were found to be much more probable in the aftermath of intense storms relative to moderate storms. It was finally shown that the average frequencies of Pc1 pulsations were higher than normal in the recovery phase of storms, and that these frequencies increased and occupied larger LT regions with increasing storm intensity.

[36] The above observations support the hypothesis that the EMIC source region moves, or extends down to lower L -shells with increasing storm intensity, producing higher-frequency EMIC waves, and decreasing the latitude at which the EMIC waves enter the ionospheric waveguide [Heacock and Kivinen, 1972]. The lower entry latitude implies a shorter propagation path to the receiver, which results in smaller overall attenuation, and hence a larger number of Pc1 observations (particularly on the dayside, where E -region attenuation is very large).

[37] **Acknowledgments.** This work was supported by QuakeFinder, LLC, Stellar Solutions Inc., the California Space Authority (CSA), and NASA grant NNG04GD16A. Magnetometer data was obtained from the Northern California Earthquake Data Center (NCEDC), contributed by the Berkeley Seismological Laboratory, University of California, Berkeley. The authors would like to thank Celeste V. Ford for her ongoing help and support. RLM would like to acknowledge support from NSF GEM ATM 02-1798 and NSF Space Weather ATM 02-08501.

[38] Zuyin Pu thanks Mark Engebretson for his assistance in evaluating this paper.

References

- Althouse, E. L., and J. R. Davis (1978), Five station observations of Pc1 micropulsation propagation, *J. Geophys. Res.*, **83**, 132–144.
- Anderson, B. J., and D. C. Hamilton (1993), Electromagnetic ion cyclotron waves stimulated by modest magnetospheric compressions, *J. Geophys. Res.*, **98**, 11,369–11,382.
- Anderson, B. J., R. E. Erlandson, and L. J. Zanetti (1992), A statistical study of Pc 1–2 magnetic pulsations in the equatorial magnetosphere: 2. Wave properties, *J. Geophys. Res.*, **97**, 3089–3101.
- Bortnik, J., J. W. Cutler, C. Dunson, and T. E. Bleier (2007), An automatic wave detection algorithm applied to Pc1 pulsations, *J. Geophys. Res.*, **112**, A04204, doi:10.1029/2006JA011900.
- Bräysy, T., K. Mursula, and G. Marklund (1998), Ion cyclotron waves during a great magnetic storm observed by Freja double-probe electric field instrument, *J. Geophys. Res.*, **103**, 4145–4155.
- Campbell, W. H., and E. C. Stiltner (1965), Some characteristics of geomagnetic pulsations at frequencies near 1 c/s, *Radio Sci. J. Res.*, **69D**, 1117–1132.
- Cornwall, J. M. (1965), Cyclotron instabilities and electromagnetic emission in the ultra low frequency and very low frequency ranges, *J. Geophys. Res.*, **70**, 61–69.
- Cornwall, J. M., F. V. Coroniti, and R. M. Thorne (1970), Turbulent loss of ring-current protons, *J. Geophys. Res.*, **70**, 4699–4709.
- Engebretson, M. J., W. K. Peterson, J. L. Posch, M. R. Klatt, B. J. Anderson, C. T. Russell, H. J. Singer, R. L. Arnoldy, and H. Fukunishi (2002), Observations of two types of Pc 1–2 pulsations in the outer dayside

- magnetosphere, *J. Geophys. Res.*, *107*(A12), 1451, doi:10.1029/2001JA000198.
- Fraser, B. J. (1968), Temporal variations in Pc1 geomagnetic micropulsations, *Planet. Space Sci.*, *16*, 111–124.
- Fraser-Smith, A. C. (1970), Some statistics on Pc1 geomagnetic micropulsation occurrence at middle latitudes: Inverse relation with sunspot cycle and semiannual period, *J. Geophys. Res.*, *75*, 4735–4745.
- Hamilton, D. C., G. Gloeckler, F. M. Ipavich, W. Stüdemann, B. Wilken, and G. Kremser (1988), Ring current development during the great geomagnetic storm of February 1986, *J. Geophys. Res.*, *93*, 14,343–14,355.
- Heacock, R. R., and M. Kivinen (1972), Relation of Pc1 micropulsations to the ring current and geomagnetic storms, *J. Geophys. Res.*, *77*, 6746–6760.
- Horne, R. B., and R. M. Thorne (1990), Ion cyclotron absorption at the second harmonic of the oxygen gyrofrequency, *Geophys. Res. Lett.*, *17*, 2225–2228.
- Jacobs, J. A. (1970), *Geomagnetic Micropulsations*, Springer, New York.
- Johnson, J. R., and C. Z. Cheng (1999), Can ion cyclotron waves propagate to the ground?, *Geophys. Res. Lett.*, *26*, 671–674.
- Kangas, J., A. Aikio, and J. V. Olson (1986), Multistation correlation of ULF pulsation spectra associated with sudden impulses, *Planet. Space Sci.*, *34*, 543–553.
- Kerttula, R., K. Mursula, T. Pikkarainen, and J. Kangas (2001a), Storm-time Pc1 activity at high and middle latitudes, *J. Geophys. Res.*, *106*, 6213–6227.
- Kerttula, R., K. Mursula, T. Pikkarainen, and J. Kangas (2001b), Effect of magnetic storm intensity on Pc1 activity at high and mid-latitudes, *J. Atmos. Sol. Terr. Phys.*, *63*, 503–511.
- Manchester, R. N. (1966), Propagation of Pc1 micropulsations from high to low latitudes, *J. Geophys. Res.*, *71*, 3749–3754.
- Manchester, R. N. (1968), Correction of Pc1 micropulsations at spaced stations, *J. Geophys. Res.*, *73*, 3549–3556.
- Mursula, K., B. J. Anderson, R. E. Erlandson, and T. Pikkarainen (1996), Solar cycle change of Pc1 waves observed by equatorial satellite and on the ground, *Adv. Space Res.*, *17*, (10)51–(10)55.
- Olson, J. V., and L. C. Lee (1983), Pc1 wave generation by sudden impulses, *Planet. Space Sci.*, *31*, 295–302.
- Perraut, S., R. Gendrin, A. Roux, and C. de Villedary (1984), Ion cyclotron waves: Direct comparison between ground-based measurements and observations in the source region, *J. Geophys. Res.*, *89*, 195–202.
- Rauch, J. L., and A. Roux (1982), Ray tracing of ULF waves in a multi-component magnetospheric plasma: Consequences for the generation mechanism of ion cyclotron waves, *J. Geophys. Res.*, *87*, 8191–8198.
- Tepley, L. (1965), Regular oscillations near 1 c/s observed at middle and low latitudes, *Radio Sci. J. Res.*, *69D*, 1089–1105.
- Thorne, R. M., and R. B. Horne (1993), Cyclotron absorption of ion cyclotron waves at the bi-ion frequency, *Geophys. Res. Lett.*, *20*, 317–320.
- Thorne, R. M., and R. B. Horne (1994), Energy transfer between energetic ring current H^+ and O^+ by electromagnetic ion cyclotron waves, *J. Geophys. Res.*, *99*, 17,275–17,282.
- Wentworth, R. C. (1964), Enhancement of hydromagnetic emissions after geomagnetic storms, *J. Geophys. Res.*, *69*, 2291–2298.

J. Bortnik and R. L. McPherron, Institute of Geophysics and Planetary Physics, University of California, Los Angeles, Room 6711, Geology Building, Los Angeles, CA 90095-1565, USA. (jbortnik@gmail.com; mcpherron@igpp.ucla.edu)

J. W. Cutler, C. Dunson, and T. E. Bleier, QuakeFinder, LLC, 250 Cambridge Avenue, Suite 204, Palo Alto, CA 94305, USA. (jwc@stanford.edu; cdunson@quakefinder.com; tbleier@quakefinder.com)